Investigation on the Wire Electric Discharge Machining Performance of artificially aged Al6061/B$_4$C composites by Response Surface Method

D. Deepak [a] , *M.C. Gowrishankar[b]**, *D. Sai Shreyas[a,b]*

[a]Manipal Institute of Technology, Department of Mechatronics, Manipal Academy of Higher Education, 576104, Manipal, India.
[b]Manipal Institute of Technology, Department of Mechanical and Industrial Engineering, Manipal Academy of Higher Education, 576104, Manipal, India.

Present research work is focused on investigation of material removal rate in Wire-ED Machining (EDM) of artificially aged Al-6061/ B$_4$C reinforced composites with 2-6 wt.% in peak aged condition. Combined effect of B$_4$C and artificial aging at 100°C improved the hardness by 20 - 170% under as cast and artificially aged condition. Initially the wire EDM experiments are conducted on Al6061 alloy and then the process parameters such as current, pulse-on time (t_{on}) and pulse-off time (t_{off}) are optimized to obtain the high material removal rate (MRR). At optimized conditions test samples with various % of B$_4$C are machined to study their influence on MRR. The study revealed that current and t_{off} had a significant influence. MRR increased as current is increased and it decreased as t_{off} is increased. Maximum MRR at optimum settings, current : 5.53 A, T_{off} : 10 µs and T_{on} : 36.46 µs is 2.45 mg/min. Considering the limitation of the experimental set up the modified optimum settings (T_{off} : 10 µs, T_{on} : 30 µs and current : 5 A) resulted in average MRR of 2.39 mg/min with deviation of 0.20 mg/min. The study showed that there is no significant difference in MRR and the morphology of the machined surface with respect to test samples of different % of B$_4$C particles as reinforcement in Al6061 composite.

Keywords: *Wire-EDM, Artificial aging, Al6061/B$_4$C composite, pulse on time, pulse off time.*

1. Introduction

Aluminium alloy and its composites exist in a variety of light alloy matrices, mainly Mg, Al, and Ti, with continuous fiber, ceramics in particle, chopped fiber, or whisker form reinforcements. Aluminum and its alloys are commonly utilised as the matrix in aluminum-based composites. SiC and B$_4$C are the preferred reinforcements in these matrices, however other materials such as TiC, Al$_2$O$_3$, and B fibres have been frequently employed in the past[1]. In recent years, these composites have mostly been used in aerospace, automotive, and marine applications. When compared to unreinforced matrix alloy systems, aluminum composites reinforced with SiC particles improve yield strength by up to 20%, have a lower thermal expansion coefficient, higher elasticity modules, and better wear resistance. When compared to other materials, B$_4$C reinforced aluminum composites are harder, tougher, more fracture-resistant, lighter in weight, have better fatigue strength, and have dramatically improved characteristics. Aluminum based composites are now replacing steel and aluminum alloy components (e.g., hydraulic cylinder, drive shafts etc.) in the field of automotive sector for weight reduction and wear resistance in essential components[2-7]. The comprehensive literature shows that boron carbide (B$_4$C) is an alternative for composites reinforced with silicon carbide (SiC) due to better interfacial bonding with matrix alloy. It is reported that interfacial bonding between the Al matrix with B$_4$C is better than that of SiC reinforced composites[7-9]. Mechanical properties of composites have improved due to uniform distribution of reinforcement and a good interface between matrix and reinforcement. SiC reinforced composites have lower strengthening effects than B$_4$C reinforced composites. Age hardening is the prominent heat treatment process used to increase specific strength of several aluminium alloys[1-3]. The primary purpose of ageing treatment of these alloys (Al-Mg-Si) is to obtain a systematically growing enormous number of uniformly distributed fine intermediate precipitates (Mg$_2$Si) in the matrix. Improvement in mechanical properties like hardness, tensile strength, and wear resistance have been extensively studied under both as cast and heat-treated conditions. Machining of such reinforced composite is challenging due to hard and abrasive nature of reinforced particles. The major challenges are considerably high-power requirement, high surface roughness, poor machinability, high tool wear and tool costs[10-13]. In view of this, the wire-EDM is suitable method for machining of electrically conductive materials. In this process, material is removed due to high frequency repetitive sparks which occur between workpiece and tool. This leads to localized raise in temperature in the spark gap which melt and vaporize the material. The circulation of dielectric, regulated the electrical discharge and take the debris of machining away[14]. In recent days, this process is used for production of nozzles, miniatured holes for cooling

*e-mail: gowri.shankarmc@manipal.edu

turbine blades, biomedical and micro-electro-mechanical devices[15] and polishing of 3D printed parts[11]. The polished 3D printed SS316L resulted in removal of defects such as porosity, the balling pits and voids. The settings to the wire-EDM process parameters show significant influence on MRR, surface roughness and kerf width. The high t_{on} create prolonged discharge and results in higher surface roughness. The smaller SiC of size 0.7–13 μm did not show considerable difference on the surface quality and also, they resulted in bigger kerf width and lower tool wear compared to generated by larger sized particles. Use of the multiwalled carbon nanotubes (1 g/L) in the dielectric fluid improved MRR by 75.42%, reduced roughness of the machined surface by 19.15% and recast layer thickness as well as other surface defects in machining of Nitinol shape memory alloy[16]. Studies of zinc coated copper wire showed that electrical parameters such as capacitance and voltage, and machining parameters such as feed rate exhibited prominent combined effect on the surface roughness and kerf-width[17]. In general, increase in current and t_{on} resulted in improving the MRR[18-21]. The dielectric fluid mixed with conductive powder produced a stable and higher electric discharge resulting in improved machining performance[22]. However, a comparative study of electrode wear showed that a significant amount to material transfer occur by copper electrode compared to the graphite. The increase in t_{on} and current resulted in increase of electrode wear and surface roughness of Al (6351)-SiC-B_4C composite due to production of larger craters[23]. Ramulu and Taya[24] investigated the EDM characteristics of Al/SiC$_w$ composites and it was found that MRR and surface roughness were higher for SiC$_w$ 15% reinforced composite. The current is found significantly influence the surface finish and the effect of voltage as well as t_{on} was insignificant[25]. Also, the percentage of ceramic reinforcement and t_{on} were found to be significant on surface finish and kerf width. The higher reinforcement content in the matrix material reduce the machining speed[26]. Sushant Dhar et al.[27] developed a model for predicting MRR, tool wear rate and over cut for EDM of Al–4Cu–6Si alloy–10 wt.% SiC$_p$ composites. Bassam Khan et al.[28] investigated the effect of T_{on}, T_{off}, wire feed rate and its tension, voltage, current and fluid pressure on surface roughness obtained on Ti-6Al-4V Grade-5 alloy. Study showed that cryogenic machining resulted in improving the machinability. The settings to the process parameters such as current, T_{on}, T_{off}, spark gap voltage showed significant influence on surface roughness of the cut surface.

Rahul Davi et al.[29] made a detailed review of effect of EDM process parameters on machining and also investigated the effect of tool geometry on the machining characteristics of SiC powder mixed hybrid metal matrix composite by EDM for drilling purpose. It was found that both material removal and tool wear rate increased with increase in current and the duty-factor for electrodes of cylindrical and conical geometries due to higher spark energy. Comparatively, the hollow cylindrical copper tool produced higher MRR compared to solid conical tool by 33.79%.

Machining of particle reinforced aluminum composite by traditional techniques shows challenges such as micro-cracks, pits formation, voids, high tool wear-rate and embedment of fractured particles on the cut surface. The machining quality greatly influence the performance of material in applications. Few of these challenges can be solved by wire-EDM. Literature show that there is a lack of information on the effect of B_4C particles in Al6061 composite with respect to MRR and its surface morphology during wire-EDM. This paper investigates the effects of crucial parameters on MRR, such as current, t_{on}, and t_{off}, and develops optimal settings to enhance productivity in terms of MRR and establish regression model to predict MRR by using response surface method. Further, the effect of wt.% of B_4C particles upto 6% on machining is also investigated.

2. Methodology

2.1. Preparation of B_4C particles for fabrication

B_4C particles are cleaned with distilled water in an ultrasonic agitator to cleanse its surface as well as to remove sedimented fine particles. Agitation process is performed 4 times for 10-15 min with distilled water. Water is to be decanted after each agitation and fresh water is to be used for the next stage. After cleaning the reinforcement particles with distilled water, it is to be cleaned once again with acetone by ultrasonic agitation. Acetone is then decanted and powder particles are dried. To eliminate volatile compounds, B_4C particles were preheated at 250°C/2 h. Particle agglomeration will be formed if B_4C is preheated above 300°C because of formation of boric oxide (B_2O_3) layer. Preheating B_4C particles removes surface impurities and improves wettability of the reinforcements[30].

2.2. Preparation of Al6061-B_4C composite

Table 1 shows composition of matrix material (Al6061) and Table 2 shows properties of Al6061 alloy and B_4C reinforcements. Figure 1a, b shows fabrication process of test samples. The reinforcement particles of size 35-40 μm (400 Mesh) are procured from Boron Carbide India limited, Mumbai. Scanning Electron Microscopy (SEM) and Energy Dispersive X-ray spectroscopy (EDAX) of B_4C were used for the present work shown in Figure 1c, d. Al6061 billets are melted in a graphite crucible using a 5 kW electric resistance furnace, and the melting process is allowed to continue until a consistent temperature of 750°C is reached. Scum powder (small quantity) is added to the melt to remove floating slag. By adding dry hexachloroethane (C_2Cl_6-10gms) tablet molten melt is degassed[31].

The melt is then allowed to cool to a semi-solid state at 600°C (just below the liquidus temperature). The preheated B_4C (2, 4 and 6 wt.%) is slowly introduced into vortex of molten metal developed during continuous stirring at 150-200 rpm for duration of 10 min. After mixing reinforcements in semisolid state, composite slurry is reheated and kept at 750°C and stirring is repeated for 10 min at 400 rpm to obtain uniform distribution of B_4C particles in the matrix. Melt is poured into preheated cast iron moulds which are maintained at temperature of 500°C. Artificial aging is performed on cast samples by solutionizing at 558°C/2 h, then quenching in demineralised water at 25°C. Now samples are artificially aged in furnace at 100°C/8 h to achieve maximum hardness[30]. To measure hardness of alloy and

Investigation on the Wire Electric Discharge Machining Performance of artificially aged Al6061/B$_4$C composites by Response Surface Method

3

Table 1. Composition (wt.%) of Al6061.

Material	Si	Fe	Cu	Mn	Zn	Ti	Mg	Cr	Al
wt.% (Actual)	0.50	0.55	0.25	0.14	0.24	0.12	0.95	0.20	Bal.
wt.% (Standard)	0.40 - 0.80	0.70 Max.	0.15 –0.40	0.15 Max.	0.25 Max.	0.15 Max.	0.80 –1.20	0.04 –0.35	Bal.

Table 2. Properties of Al6061 alloy and B4C reinforcements.

Properties	Al6061	B$_4$C
Hardness (HB 500)	30 BHN	3000 kg/mm^2 (30 GPa)
Poisson's Ratio	0.33	0.207
Elastic Modulus (GPa)	70-80	480
Density (g/cc)	2.7	2.52
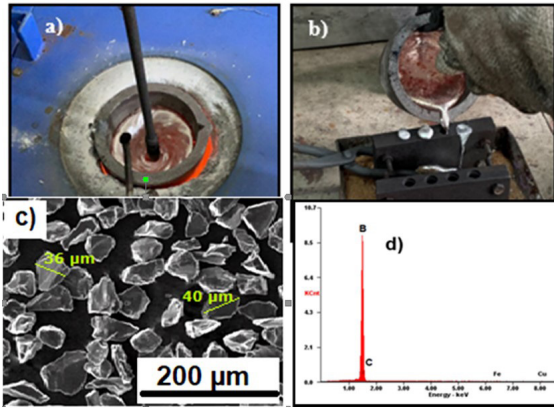
Figure 1. (a) Stirring process (b) Pouring of molten metal into pre-heated die c) SEM micrographs of B$_4$C reinforcements d) EDAX of B$_4$C reinforcements.

composites Micro Vickers Hardness Tester, Model – MMT X 7A was used with 200 gmf load and 15 seconds dwell time. Before performing hardness test all the samples were polished using disc polishing system with a velvet cloth impregnated with diamond paste, so that oxide layer and other impurities produced during heat treatment can be removed. The average of a minimum of five near identical indentation readings are noted down for each specimen at different locations of the test samples.

2.3. Density measurement

The presence of porosity, as well as its size and distribution in the matrix, is critical in determining the mechanical properties of composites. Porosity levels should be minimum in order to obtain better performance in the applications. Porosity occurs due to formation of air bubbles which enter the slurry during the stirring process. Table 3 shows theoretical and experimental density values of Al6061 alloy and B$_4$C reinforced composites. It is observed that the maximum porosity in the test samples is less than generally acceptable levels of 2-4%[32,33] porosity of the cast composites and confirms the suitability of the test specimens with minimal casting defects for further investigations. Also, it is found that the porosity

got increased with increase in B$_4$C addition to the matrix. This resulted in improvement in nucleation sites for strain hardening during age hardening process[3,6]. From Table 3 it is observed that for varied wt.% of reinforcements, theoretical and experimental densities are close to one other. Density of composite is marginally lower than base Al6061 alloy matrix. Addition of reinforcement particle (B$_4$C) having lower density compared to that of matrix (Al6061) has led to decrease in overall density of composites.

"The theoretical density is calculated by the rule of mixture as follows:

- Density of Al6061-B$_4$C composites is given by[32,33],

$$\rho_{Al6061-B4C} = Vol_{f\,Al6061} \times \rho_{Al6061} + Vol_{f\,B4C} \times \rho_{B4C}$$

Where, ρ_{Al6061} = Density of Al6061 alloy (2.7g/cc)
ρ_{B4C} = Density of B$_4$C (2.52g/cc)
$Vol_{f\,Al6061}$ = Volume fraction of Al6061 alloy
$Vol_{f\,B4C}$ = Volume fraction of boron carbide

Experimental values are calculated by weighing the sample and dividing it by volume of respective samples. Samples of 15 mm diameter and 20 mm height are prepared and volume is calculated. The experimental density value is calculated as follows",

$$\rho_{Exp} = Weight\ of\ sample\ /\ volume\ of\ sample$$

The porosity percentage is given by:

$$\%\ Porosity = [(\rho_T - \rho_{Exp})\,/\,\rho_T]\times 100\%$$

Where, ρ_T = Theoretical density and
ρ_{Exp} = Experimental density

2.4. Experimental set up

Experiments were performed using a 2-axis (X-320 mm, Y-400 mm) computer numerically controlled wire-EDM made by Concord wire-EDM, India (Model: DK7732). Tool electrode made of molybdenum wire (diameter: 0.16 mm) is employed. As a dielectric fluid, a mixture of soft water and gel is employed. The controller has a resolution of 0.001 mm. Experimental set up is shown in Figure 2.

2.5. Design of experiment

Effect of process parameters such as wire speed, voltage, t$_{off}$, t$_{on}$ and current on machining of Al6061-SiC composite was investigated by the authors earlier and these parameters were optimized[34,35]. In this work the critical parameters such as t$_{on}$, t$_{off}$ and current were chosen by setting the voltage and wire speed levels as constant. Table 4 shows the wire-EDM process parameters and their levels. These levels are chosen based on the confirmation experiments by the authors for machining of similar base metal with different reinforcing material. During the experiments, the specimen thickness

Table 3. Density value comparisons of Al6061- B_4C.

Density (g/cc)	wt. % of B_4C reinforcement			
	0% (Base)	2%	4%	6%
Theoretical Density (ρ_{the})	2.70	2.6964	2.6928	2.6892
Experimental Density (ρ_{exp})	2.6728	2.6541	2.6401	2.6174
Percentage Porosity	1.007	1.568	1.96	2.669

Table 4. Wire-EDM process parameters and their levels.

Parameters	Unit	Level 1	Level 2	Level 3
Toff	μs	10	15	20
Ton	μs	30	40	50
Current	A	4	5	6

Figure 2. Experimental setup.

and supply pressure of dielectric fluid were kept constant. The experiments are designed using L_{20} response surface method using central composite design. The design consists of 3 factors, with total 20 base runs and two blocks. The Cube points were 16, Center points in cube 12, Axial points were 12 and center points in axial is 0. Two-level, Full factorials were used for designing the experiments with two replications as shown in Table 5.

2.6. Measurement of MRR

Test samples are machined as per experimental design shown in Table 5. During machining, the MRR acquired for each trial is determined using the weight loss technique, as described by the Equation 1. A digital mass balance is used to determine weight of work piece before (W_i) and after (W_f) machining (accuracy: 0.001g). The machined sample surfaces is shown in Figure 3.

$$MRR = \frac{W_i - W_f}{t} \ mg/s \tag{1}$$

2.7. Morphological study

Optical and scanning electron microscopy (SEM) is used for morphological study of test samples. Dispersion of reinforcement in matrix alloy is investigated using SEM (Model: JEOL JSM 840A). The samples are finely polished, buffed and etched with Keller's reagent (1.0 ml-HF, 1.5 ml-HCl, 2.5 ml-HNO$_3$ and 95ml-H$_2$O) to identify B_4C reinforcement in the matrix. The morphology of the wire-ED machined surface is studied using Inverted metallurgical microscope (Model: IM 7000, Mitutoyo) at different magnifications.

Table 5. Experimental plan.

Std Order	Run Order	Pt Type	Blocks	Current (A)	t_{on} (ms)	t_{off} (ms)
2	1	1	1	6	30	10
3	2	1	1	4	50	10
17	3	0	1	5	40	15
5	4	1	1	4	30	20
8	5	1	1	6	50	20
11	6	-1	1	5	30	15
15	7	0	1	5	40	15
9	8	-1	1	4	40	15
10	9	-1	1	6	40	15
7	10	1	1	4	50	20
20	11	0	1	5	40	15
18	12	0	1	5	40	15
19	13	0	1	5	40	15
6	14	1	1	6	30	20
14	15	-1	1	5	40	20
13	16	-1	1	5	40	10
1	17	1	1	4	30	10
4	18	1	1	6	50	10
16	19	0	1	5	40	15
12	20	-1	1	5	50	15
38	21	0	2	5	40	15
36	22	0	2	5	40	15
35	23	0	2	5	40	15
40	24	0	2	5	40	15
31	25	-1	2	5	30	15
27	26	1	2	4	50	20
30	27	-1	2	6	40	15
32	28	-1	2	5	50	15
28	29	1	2	6	50	20
33	30	-1	2	5	40	10
23	31	1	2	4	50	10
22	32	1	2	6	30	10
26	33	1	2	6	30	20
21	34	1	2	4	30	10
29	35	-1	2	4	40	15
39	36	0	2	5	40	15
24	37	1	2	6	50	10
37	38	0	2	5	40	15
34	39	-1	2	5	40	20
25	40	1	2	4	30	20

3. Results and Discussion

3.1. Distribution of reinforcement in the test samples

The dispersion of reinforcements of various compositions (2, 4 and 6 wt. %) in the metal matrix is shown in Figure 4a-c.
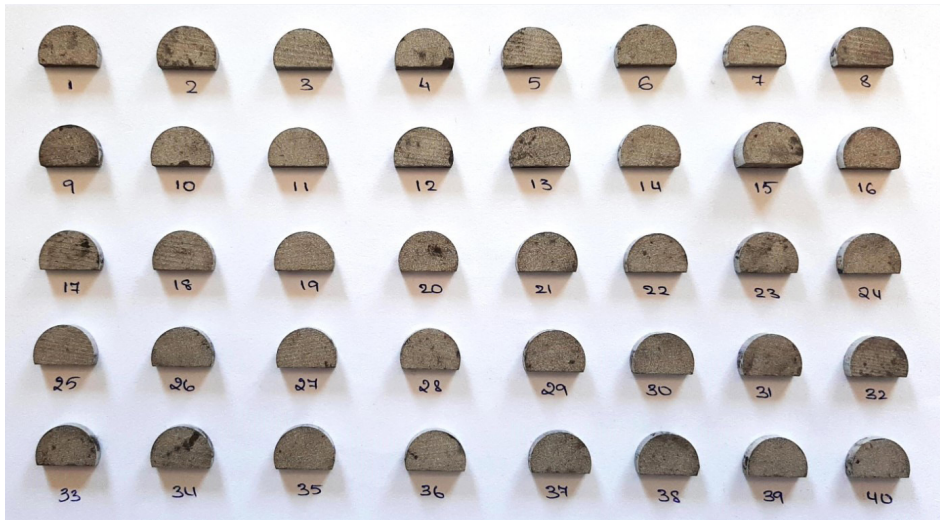
Investigation on the Wire Electric Discharge Machining Performance of artificially aged Al6061/B₄C
composites by Response Surface Method

5

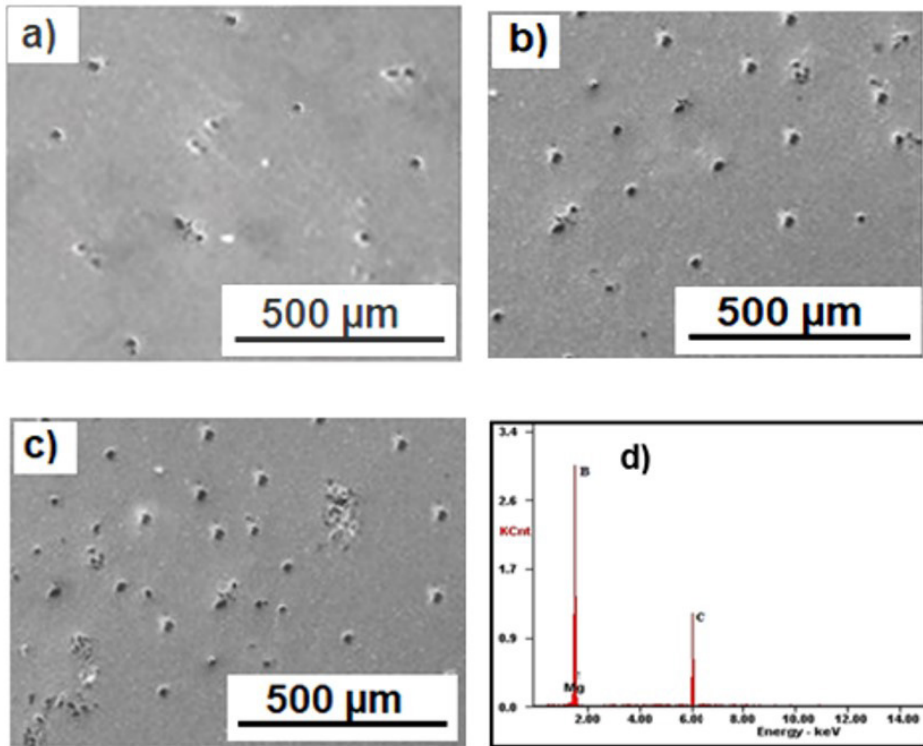**Figure 3.** Wire-ED machined test samples.

Figure 4. Dispersion of reinforcements in test samples Al6061 alloy with (a) 2% B$_4$C (b) 4% B$_4$C and (c) 6% B$_4$C composites (d) Mineral composition of the reinforced B$_4$C particle

Figure 4d shows the mineral composition of the reinforced B$_4$C particle. This examination is critical due to the fact that the mechanical property of composite is significantly influenced by particle distribution. It is seen from the figure that there is uniform distribution of reinforcements in matrix. Also, SEM images clearly indicate that the test samples are free from particle agglomeration, and blow holes or air pockets. In addition, the surface also exhibits minimal porosity in all the test samples.
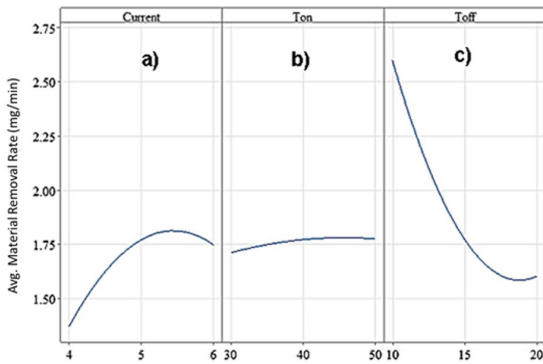
3.2. The effect of process on MRR

Figure 5 shows the effect of current, t_{on} and t_{off} on MRR. It is observed that increase in current from 4 to 5 A increased MRR due to increase in spark energy (Es)[35,36]. Higher the Es, more the material is melted and vaporized[37-39] leading to higher MRR. Further, increase in current beyond 5 A reduced the MRR after reaching a peak value in between 5 to 6 A. This indicated that, the increase in current beyond the peak current values did not yield the MRR significantly.

Change in current form 4 to 5 A resulted in increase in MRR by 13.45%, but its change from 5 to 6 A increased the MRR by 8.40%. Further, the effect of t_{on} is shown in Figure 5b. It is noticed that MRR marginally increased when t_{on} is increased. Change in t_{on} from 30 to 50 µs resulted in increase of MRR by 3.54%. The energy (E) of each spark is given by E = t_{on} × I × V. In each spark cycle as the spark duration is more the spark energy produced is also more, resulting in melting of material with greater crater size. MRR is directly proportional to crater radius. Beyond 40 µs, MRR remains almost constant. This might be due to recasting of molten pool surrounding the craters as a result of the prolonged cycle period. The effect of t_{off} on MRR is shown in Figure 5c. Increase in t_{off} time from 10 to 20 µs resulted in decrease in MRR. Interestingly, increase in t_{off} from 10 to 15 µs resulted in a sharp decrease of MRR by 28.32%. But further increase in t_{off} from 15 to 20 µs showed slightly lower rate of decrease in MRR., i.e 18.19%. t_{off} is the duration of time at which capacitors gets charged during which no sparks occur. During this period deionization of the dielectric fluid also occurs which means the machining does not occur during t_{off} period[37]. As a result, raising the t_{off} increases the cycle duration while lowering the spark frequency, resulting in a decrease in MRR.

3.3. Analysis of variance of MRR

Effect of process parameter on MRR is analyzed using ANOVA method to find effect of each control parameters.

Figure 5. The effect of a) current on MRR b) ton on MRR c) toff on MRR.

The significance of these parameters' effect are determined by conducting an F-test with a confidence level of 95% as shown in Table 6.

It is observed from Table 6 that *F* calculated is greater than $F(\alpha=.005,29)$ fo2r the machining parameters such as current and t_{off}. Hence the effect of these parameters are highly significant, a small change in settings of current and t_{off} results in significant variations to MRR. But, F values of t_{on} is less than critical values i.e., F = 0.52, which indicate changes in settings of t_{on} 30 to 50 A do not significantly alter MRR. Considering the energy efficient usage, the lower settings of current i.e., 30 A is suggested as viable setting. Further, interaction effect of t_{off} * t_{on}, t_{on} x current and t_{off} x current is shown through surface plots in Figure 6a, 6b and 6c respectively.

From the F test on these interaction effect it is seen that the interaction of t_{on} x t_{off}, t_{off} x current (pooled F values=0.12) is not significant and the variations to settings can be made independently. But the interaction between t_{on} x current has marginal influence on MRR. It means the effect of current on MRR changes with changes in settings of t_{on} and vice versa. The significance of the lack of fit is also tested through F-Test as shown in Table 6 and it is seen that its F values are less than the F critical values indicating its effect as insignificant.

3.4. Optimization of the process parameters

Response surface method is adopted for optimization of machining settings that result in higher MRR while wire-EDM of Al6061 alloy. The corresponding optimization plot of MRR is shown in Figure 7. From figure, maximum MRR is obtained by settings, current-5.53 A, t_{on} - 36.46 µs and t_{off} − 10 µs. MRR predicted at this setting is 2.45 mg/min. However considering the limitation in the settings of the experimental set up confirmation experiments were carried out at t_{off} − 10 µs, t_{on} - 30 µs and current-5 A which resulted in average MRR of 2.39 mg/min with deviation of 0.20 mg/min.

3.5. Regression modelling of MRR

A regression model is developed to establish relationship between process parameters (Ic: Current, t_{on}: Pulse-on time, t_{off}: Pulse-off time) and the response parameter MRR. Main effect, interaction effect and their squared terms of these parameters are considered in the regression modelling. The developed predictive model is given by Equation 2.

Table 6. ANOVA of MRR.

Source	DF	Adj SS	Adj MS	F-Value
Current	1	1.4268	1.4268	17.64
t_{on}	1	0.0420	0.0420	0.52
t_{off}	1	10.1235	10.1235	125.19
Current*Current	1	0.5076	0.5076	6.28
t_{on} * t_{on}	1	0.0090	0.0090	0.11
t_{off} * t_{off}	1	1.2149	1.2149	15.02
Current* t_{on}	1	0.2029	0.2029	2.51
Current* t_{off}	1	0.0062	0.0062	0.08
t_{off} * t_{on}	1	0.0031	0.0031	0.04
Lack-of-Fit	19	0.9190	0.0484	0.34

Investigation on the Wire Electric Discharge Machining Performance of artificially aged Al6061/B₄C
composites by Response Surface Method

7

The coefficients of determination (R^2) for this equation is 85.32%. Confirmation experiments within the range of operational parameters are used to assess the predicting accuracy of the regression model, that is, 10 µs ≥ t_{off} ≤ 20 µs; 30 µs ≥ t_{on} ≤ 50 µs; 4 A ≥ I ≤ 6 A. The distribution of residuals is shown in Figure 8a-d. It is seen from the Figure 8a that residuals are very close to line of fit and they show normal distribution as shown in Figure 8b. However, one of the test results show the large deviation which form the outlier data set. The scatter plot shown in Figure 8c show that residuals are distributed randomly over line of fit. These figures indicate the confirmation of model adequacy tests. Figure 8c show the standardized residual error of MRR for each experiment. It is observed that the outlier data set is

due to the experiments at settings predicted by regression model and the experimental results.

$$MRR = -2.27 + 2.670I_c + 0.0623T_{on} - 0.488T_{off} -$$
$$0.2127I^2_c - 0.000283T^2_{on} + 0.01316T^2_{off} - \quad (2)$$
$$0.00788I_c \times T_{on} - 0.0028I_c \times T_{off} + 0.00020T_{on} \times T_{off}$$

3.5. The effect B_4C content on MRR

The Al6061 composite is reinforced with B₄C particles upto 6% and further, its wire - ED machinability with respect to material removal rate is determined by machining these test samples at established optimum settings i.e., t_{off} – 10 µs, t_{on} - 30 µs and current-5 A. Figure 9 shows the MRR obtained
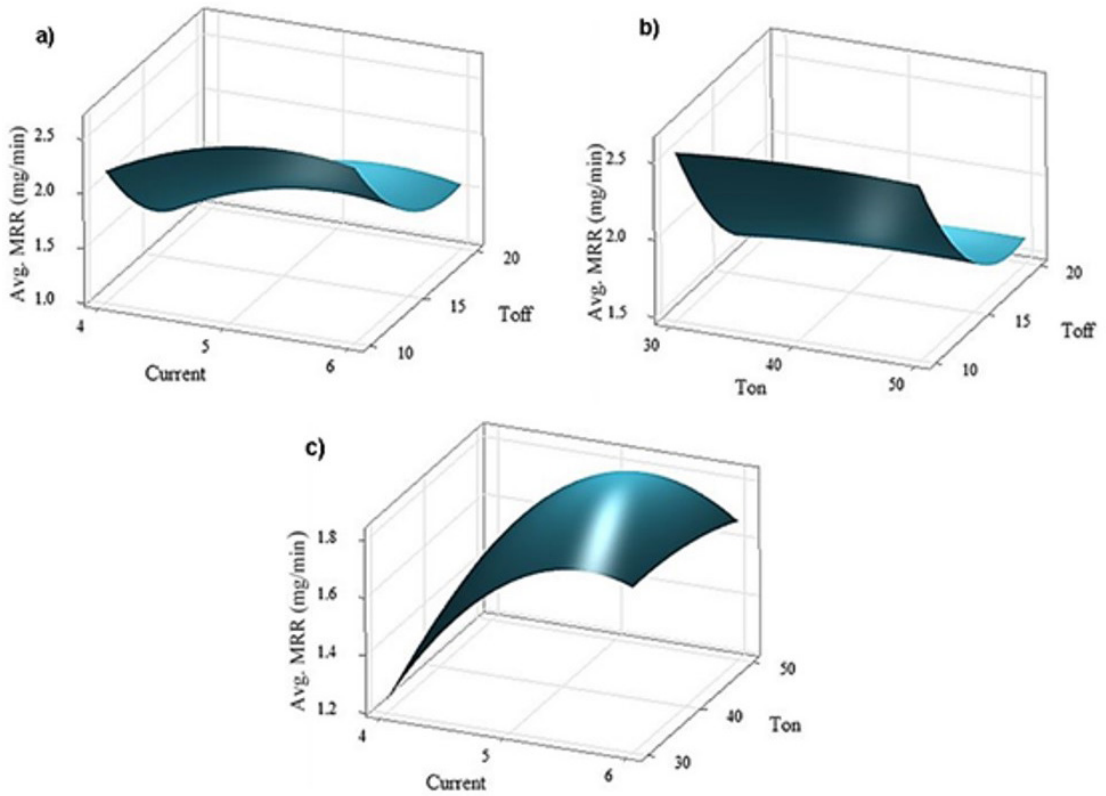

Figure 6. Interaction effect of (a) t_{off} x current (b) t_{on} x t_{off} (c) t_{on} x current.
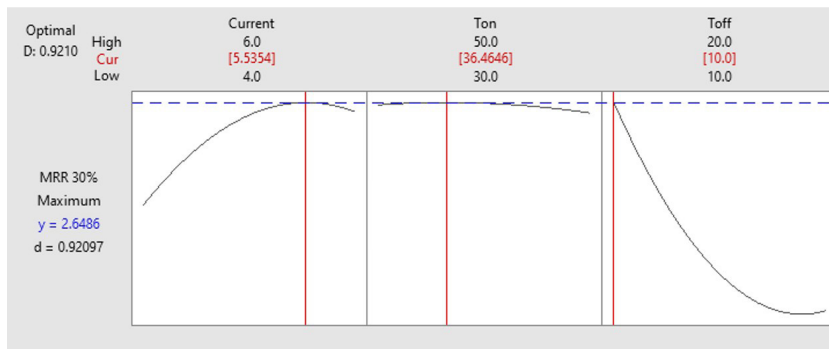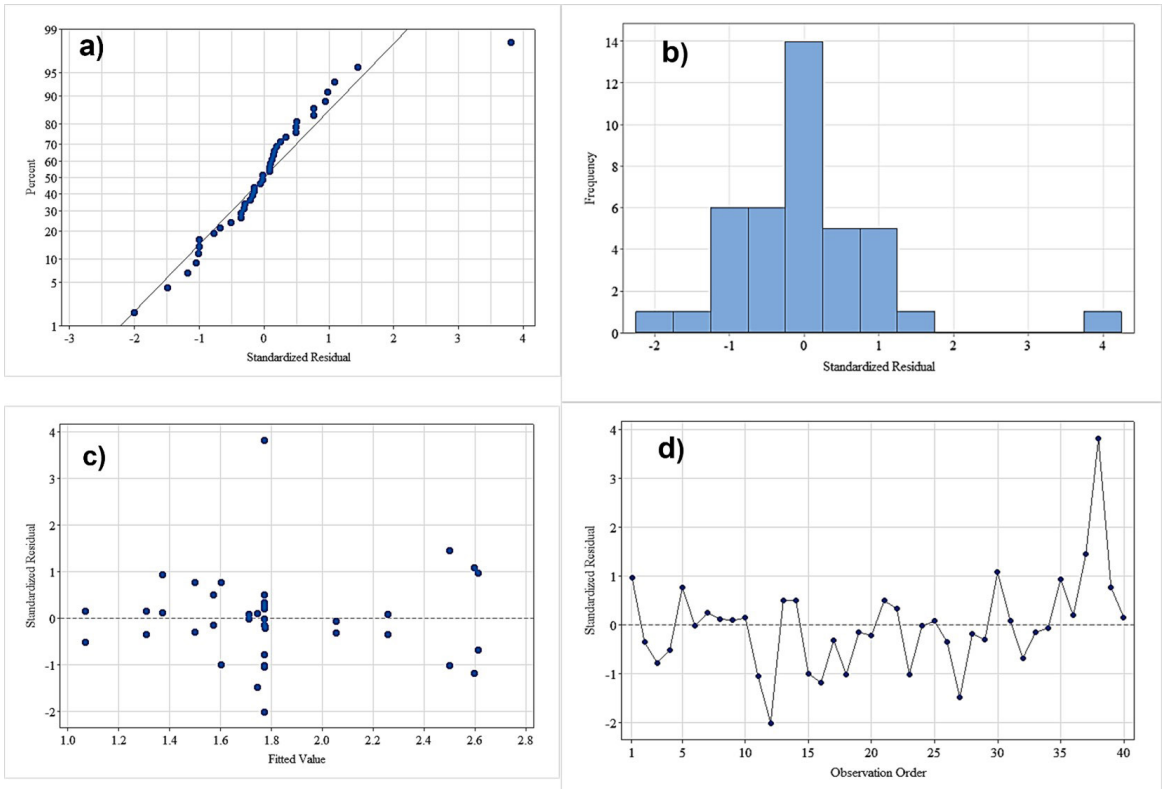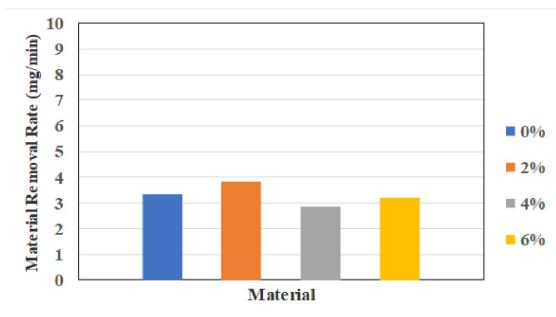

Figure 7. The optimization plot of MRR.

Figure 8. The distribution of residuals a) linear plot b) histogram plot c) scatter plot d) residual over experimental trial.

Figure 9. MRR of Al6061 alloy with 0% to 6 wt. % B_4C particle reinforced composite.

by Al6061 test samples with 0, 2, 4 and 6 wt.% B_4C particles. It is observed that there is slight decrease MRR in these test samples with B_4C particles, however, the decrease in MRR is not significant. The small variation observed in the Figure 9 is mainly due to heterogeneous nature of the composite material.

Further the morphology of machined surfaces is carried out on the samples machined at optimum conditions. Figure 10a-d shows the cut surfaces of 0 – 6% B_4C composite as seen by the optical microscope and the Figure 11a-d shows the SEM images which show the micro-structure of the wire-EDM Al6061 with 6% B_4C particle composite. It is observed that the machined surfaces are characterized by uneven surfaces. This is mainly due to repeated melting and solidification of the localized regions of the machining zone which is exposed

to high temperature. However, no specific difference in the patterns of the surface morphology is seen on the machined surfaces with different % of B_4C particles as seen in these figures. Also due to sudden cooling of the molten pool during toff, the surface cracks were seen to be developed as shown in Figure 11b and c. Due to the movement of the travelling wire over the molten pool, the surface is also seen to be distorted and forming the wear tracks as seen these figure.

As shown in Table 7, the hardness of the test samples increased with increase in wt.% of B_4C particles, resulting in larger dislocation densities during solidification due to thermal mismatch between matrix alloy and reinforcement. This causes significant internal stresses and mismatch strain, which have an impact on microstructure and mechanical properties of composites. Matrix deforms plastically to meet reinforcement particles' smaller volume expansion, resulting in greater dislocation density. Increased dislocation density result in greater resistance to plastic deformation and an increase in composite hardness[1-3]. As-cast Al6061 alloy had a VHN of 60, but as-cast Al6061- B_4C (1, 2, and 3 wt.%) composites had 70, 75, 84 VHN respectively, whereas artificially aged Al6061 alloy and its composite samples show hardness of 75, 128, 136 and 144 VHN respectively. The presence of reinforcement and aging effect at 100°C resulted in improving the hardness of the test material by about 20-140% compared to Al6061 alloy. Because of the difference in thermal co-efficient of expansion between matrix and reinforcements, presence of harder reinforcements in matrix accelerates the ageing kinetics during artificial aging[3].
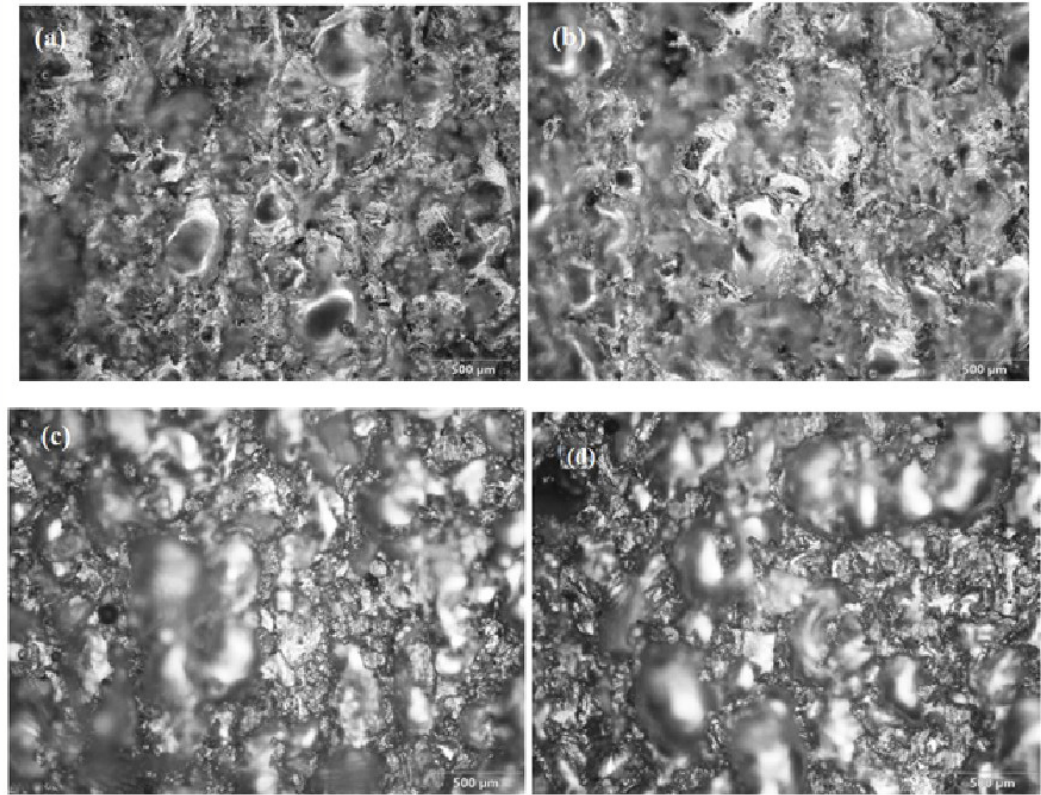
Investigation on the Wire Electric Discharge Machining Performance of artificially aged Al6061/B$_4$C composites by Response Surface Method

9

Figure 10. (a) - (d) Surface morphology of 0 to 6 wt.% B$_4$C particle reinforced composite by optical microscope.
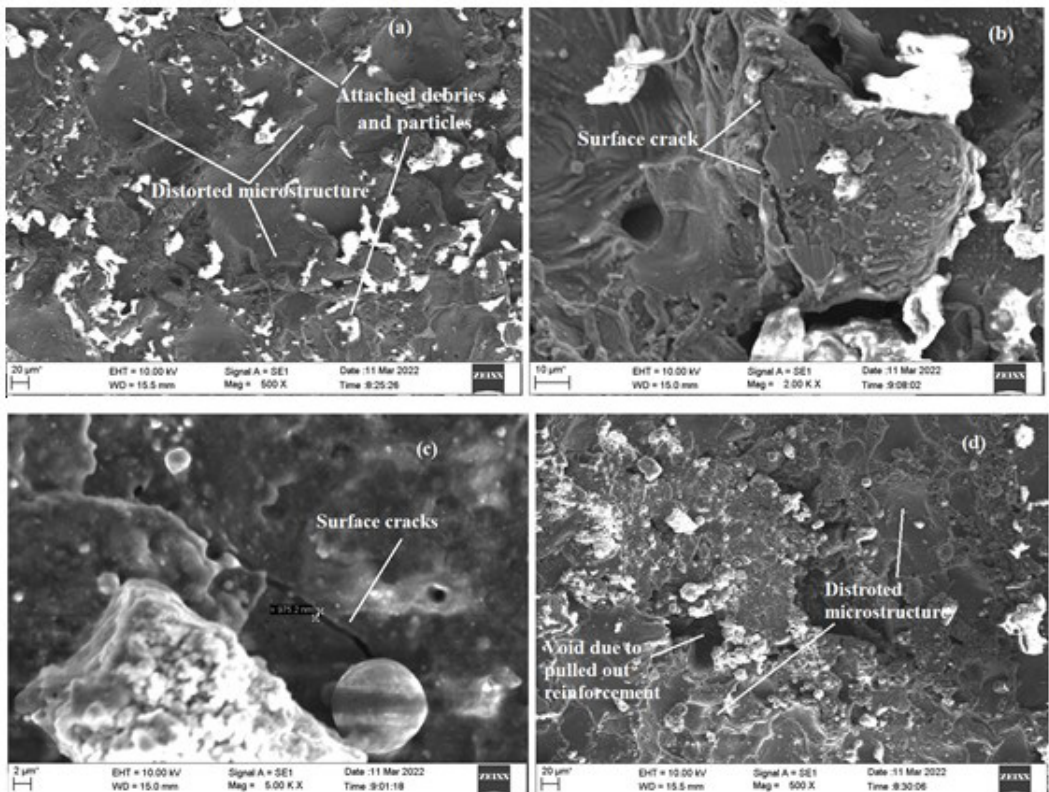

Figure 11. (a-d) Surface morphology of wire EDM surface of Al6061-B$_4$C composite (6%).

Table 7. Hardness of Al6061- B$_4$C (0, 2, 4 and 6% wt.) as cast and peak aged condition.

	As cast condition (BHN)	Peak aged condition at 100°C (BHN)
Al6061 alloy	60	95
Al6061- 2% B$_4$C	70	128
Al6061- 4% B$_4$C	75	136
Al6061- 6% B$_4$C	84	144

This may lead to surface cracks on the machined surfaces as seen in the Figure 10. Due to very high temperature involved in wire EDM process, it is observed that microstructure of the machined surfaces is distorted compared to unmachined surfaces.

4. Conclusions

This paper investigated the effect of crucial parameters such as current, t$_{on}$ and t$_{off}$ on MRR and determined the optimal settings to enhance MRR while wire-EDM of upto 6 wt.% B$_4$C particle reinforced Al6061 alloy. The data generated by this research is helpful in machining of drive shafts in aerospace and automobile industry for selecting the optimum process settings for machining of aluminum composites. The following conclusion are drawn based on the wire-EDM of upto 6 wt.% B$_4$C particle reinforced Al6061 alloy.

- SEM microstructural analysis reveals homogeneous dispersion of B$_4$C particles in alloy matrix and as compared to Al6061 matrix alloy, 20-40% and 60-140% increase in hardness is seen in as cast and aged samples at 100°C for a significant period of time.
- MRR was significantly influenced by process parameters such as current and t$_{off}$. With increasing current and decreasing t$_{off}$ in settings, the MRR increased: 4 A ≥ I ≤ 6 A; 30 µs ≥ t$_{on}$ ≤ 50 µs; 10 µs ≥ t$_{off}$ ≤ 20 µs.
- The maximum MRR is predicted at optimum settings, current-5.53 A, t$_{on}$ - 36.46 µs and t$_{off}$ – 10 µs is 2.45 mg/min. Considering the limitation in the settings of the experimental set up the modified optimum settings (current-5 A, t$_{on}$ - 30 µs and t$_{off}$ – 10 µs) resulted in average MRR of 2.39 mg/min with deviation of 0.20 mg/min.
- Within the working range, regression models are created to predict the MRR (4 A ≥ I ≤ 6 A; 30 µs ≥ t$_{on}$ ≤ 50 µs; 10 µs ≥ t$_{off}$ ≤ 20 µs) with average R^2 - 85.65%.
- The addition of B$_4$C particles to Al6061 alloy up to 6 wt.% did not have a significant effect on the MRR and morphology of the wire EDM machined surface.

5. References

1. Gowrishankar MC, Hiremath P, Shettar M, Sharma S, Satish Rao U. Experimental validity on the casting characteristics of stir cast aluminium composites. J Mater Res Technol. 2020;9(3):3340-7.
2. Srinivas D, Gowrishankar MC, Hiremath P, Shettar M, Jayashree PK. Influence of various trace metallic additions and reinforcements on A319 and A356 alloys- A review. Cogent Engineering. 2022;9(1):2007746.
3. Shettar M, Hiremath P, Shankar G, Kini A, Sharma S. Tribolayer behaviour and wear of artificially aged Al6061 hybrid composites. Int J Automot Mech Eng. 2021;18(2):8668-76.
4. Baradeswaran EP. Influence of B$_4$C on the tribological and mechanical properties of Al 7075-B$_4$C composites. Composites. 2013;54:146-52.
5. Previtali B, Pocci D, Taccardo C. Application of traditional investment casting process to aluminium matrix composites. Composites. 2008;39:1606-17.
6. Nieh TG, Karlak RF. Aging characteristics of B$_4$C-reinforced 6061-Aluminium matrix. Scr Metall. 1984;18:25-8.
7. Toptan F, Kilicarslan A, Karaaslan A, Cigdem M, Kerti I. Processing and microstructural characterisation of AA1070 and AA6063 matrix B$_4$C reinforced composites. Mater Des. 2010;31:87-91.
8. Mahesh VP, Nair PS, Rajan TPD, Pai BC, Hubli RC. Processing of surface treated boron carbide-reinforced aluminium matrix composites by liquid-metal stir-casting technique. J Compos Mater. 2011;45(23):2371-8.
9. Onoro J, Salvador MD, Cambronero LEG. High-temperature mechanical properties of aluminium alloys reinforced with boron carbide particles. Mater Sci Eng. 2010;499:421-6.
10. Knowles AJ, Jianga X, Galano M, Audebert F. Microstructure and mechanical properties of 6061 Al alloy based composites with SiC nanoparticles. J Alloys Compd. 2014;615:401-5.
11. Songmene V, Khettabi R, Zaghbani I, Kouam J, Djebar A. Machining and machinability of aluminum alloys. In: Kvackaj T. Aluminium alloys, theory and applications. London: IntechOpen Limited; 2011.
12. Sarikaya M, Gupta MK, Tomaz I, Danish M, Mia M, Rubaiee S, et al. Cooling techniques to improve the machinability and sustainability of light-weight alloys: a state-of-the-art review. J Manuf Process. 2020;62:179-201.
13. Rahman A, Ahmed A, Mia M. Trends in electrical discharge machining of Ti and Ni-based superalloys: macro-micro-compound arc/spark/melt process. In: Saleh T, Ali MSM, Takahata K, editors. Micro electro-fabrication: micro and nano technologies. USA: Elsevier; 2021. p. 63-87.
14. Nair SV, Tien JK, Bates RC. SiC-reinforced aluminium metal matrix composites. International Metals Reviews. 2013;30:275-90.
15. Kulkarni VN, Gaitonde VN, Karnik SR, Manjaiah M, Paulo Davim J. Machinability analysis and optimization in Wire-EDM of medical grade NiTiNOL memory alloy. Materials (Basel). 2020;13:2184-201.
16. Chaudhari R, Khanna S, Vora J, Patel VK, Paneliya S, Pimenov DY, et al. Experimental investigations and optimization of MWCNTs-mixed WEDM process parameters of nitinol shape memory alloy. J Mater Res Technol. 2021;15:2152-69.
17. Sivaprakasam P, Hariharana GS. Optimization of micro-WEDM process of aluminum matrix composite (A413-B4C): a response surface approach. Mater Manuf Process. 2013;28(12):1340-47.
18. Hocheng H, Lei WT, Hsu HS. Preliminary study of material removal in electrical-discharge machining of SiC/Al. J Mater Process Technol. 1997;63(1-3):813-8.
19. Singh B, Kumar J, Kumar S. Influences of process parameters on MRR improvement in simple and powder mixed EDM of AA6061/10%SiC composite. Mater Manuf Process. 2015;30:303-12.
20. Singh N, Raghukandan K. Rathina sabapathi M, Pai BC. Electric discharge machining of Al-10%SiC$_p$ as-cast metal matrix composites. J Mater Process Technol. 2004;156:1653-7.

Investigation on the Wire Electric Discharge Machining Performance of artificially aged Al6061/B$_4$C composites by Response Surface Method

11

21. Habib SS. Study of the parameters in electrical discharge machining through response surface methodology approach. Appl Math Model. 2009;33:4397-407.

22. Singh S, Bhardwaj A. Review to EDM by using water and powder-mixed dielectric fluid. J Miner Mater Charact Eng. 2011;10:199-230.

23. Kumar SS, Uthayakumar M, Kumaran ST, Parameswaran P. Electrical discharge machining of Al(6351)-SiC-B$_4$C hybrid composite. Mater Manuf Process. 2014;29(11-12):1395-400.

24. Ramulu M, Taya M. EDM machinability of SiC$_w$/Al composites. J Mater Sci. 1989;24:1103-8.

25. Hung NP, Yang LJ, Leong KW. Electrical discharge machining of cast metal matrix composites. J Mater Process Technol. 1994;44:229-36.

26. Patil NG, Brahmankar PK. Some studies into wire electro-discharge machining of alumina particulate-reinforced aluminum matrix composites. Int J Adv Manuf Technol. 2010;48:537-55.

27. Dhar S, Purohit R, Saini N, Sharma A, Hemath Kumar G. Mathematical modeling of electric discharge machining of cast Al–4Cu–6Si alloy–10 wt.% SiC$_P$ composites. J Mater Process Technol. 2007;194:24-9.

28. Khan B, Davis R, Singh A. Effect of input variables and cryogenic treatment in wire electric discharge machining of Ti-6Al-4V alloy for biomedical applications. Mater Today: Proc. 2020;27(3):2503-7.

29. Davis R, Singh A, Amorim FL, Jackson MJ, Sales WF. Effect of tool geometry on the machining characteristics amid SiC powder mixed electric discharge drilling of hybrid metal matrix composite. Silicon. 2022;14:27-45.

30. Sharma S, Kini A, Shankar G, Rakesh TC, Chaitanya K, Shettar M. Tensile fractography of artificially aged Al6061-B$_4$C composites. J Mech Eng Sci. 2018;12(3):3866-75.

31. Gruzleski JE, Closset BM. The treatment of liquid aluminium and silicon alloys. Schaumburg: American Foundry Society; 1990. p. 172-5.

32. Kok M. Production and mechanical properties of Al$_2$O$_3$ particle-reinforced 2024 aluminium alloy composites. J Mater Process Technol. 2005;161(3):381-7.

33. Prabu SB, Karunamoorthy L, Kathiresan S, Mohan B. Influence of stirring speed and stirring time on distribution of particles in cast metal matrix composite. J Mater Process Technol. 2006;171(2):268-73.

34. Kenneth KA, Ayotunde OA. Production and age-hardening behaviour of borax premixed SiC reinforced Al-Mg-Si alloy composites developed by double stir-casting technique. The West Indian J Eng. 2012;34(1):80-5.

35. Doreswamy D, Bongale AM, Piekarski M, Bongale A, Kumar S, Pimenov DY, et al. Optimization and modeling of material removal rate in Wire-EDM of silicon particle reinforced Al6061 composite. Materials (Basel). 2021;14(21):6420.

36. Lenin N, Sivakumar M, Selvakumar G, Rajamani D, Sivalingam V, Gupta M, et al. Optimization of process control parameters for WEDM of Al-LM25/Fly Ash/B$_4$C hybrid composites using evolutionary algorithms: a comparative study. Metals (Basel). 2021;11(7):1105.

37. Aggarwal V, Pruncu CI, Singh J, Sharma S, Pimenov DY. Empirical investigations during WEDM of Ni-27Cu-3.15Al-2Fe-1.5Mn based superalloy for high temperature corrosion resistance applications. Materials (Basel). 2020;13(16):3470.

38. Doreswamy D, Javeri J. Effect of process parameters in EDM of D2 steel and estimation of coefficient for predicting surface roughness. Int J Mach Mach Mater. 2018;20:101-17.

39. Deepak D, Shrinivas P, Hemant G, Iasy R. Optimisation of current and pulse duration in electric discharge drilling of D2 steel using graphite electrode. Int J Automot Mech Eng. 2018;15:5914-26.